Geophysical Research Letters

RESEARCH LETTER
10.1029/2018GL079051

Key Points:
- We compare full particle-in-cell simulations and MMS observations of magnetic reconnection with cold ions
- The perpendicular current reduction is linearly proportional to the cold ion density ratio inside the separatrix region
- The Hall electric field peak is reduced along the separatrix when cold ions are present

Supporting Information:
- Supporting Information S1
- Figure S1
- Text S1

Correspondence to:
S. Toledo-Redondo,
sergiotr@ugr.es

Citation:
Toledo-Redondo, S., Dargent, J., Aunai, N., Lavraud, B., André, M., Li, W., et al. (2018). Perpendicular current reduction caused by cold ions of ionospheric origin in magnetic reconnection at the magnetopause: Particle-in-cell simulations and spacecraft observations. *Geophysical Research Letters*, *45*, 10,033–10,042. https://doi.org/10.1029/2018GL079051

Received 1 JUN 2018
Accepted 28 JUL 2018
Accepted article online 6 AUG 2018
Published online 1 OCT 2018

Perpendicular Current Reduction Caused by Cold Ions of Ionospheric Origin in Magnetic Reconnection at the Magnetopause: Particle-in-Cell Simulations and Spacecraft Observations

Sergio Toledo-Redondo[1], Jérémy Dargent[2,3], Nicolas Aunai[2], Benoit Lavraud[3], Mats André[4], Wenya Li[4,5], Barbara Giles[6], Per-Arne Lindqvist[7], Robert E. Ergun[8], Christopher T. Russell[9], and James L. Burch[10]

[1]ESAC, European Space Agency, Madrid, Spain, [2]Laboratory of Plasma Physics - École Polytechnique, CNRS, UPMC, Université Paris-Sud, Paris, France, [3]Institut de Recherche en Astrophysique et Planétologie, Université de Toulouse, CNRS, UPS, CNES, Toulouse, France, [4]Swedish institute of Space Physics, Uppsala, Sweden, [5]State Key Laboratory of Space Weather, National Space Science Center, Chinese Academy of Sciences, Beijing, China, [6]NASA Goddard Space Flight Center, Greenbelt, MD, USA, [7]Department of Space and Plasma Physics, Royal Institute of Technology, Stockholm, Sweden, [8]Laboratory of Atmospheric and Space Physics, University of Colorado Boulder, Boulder, CO, USA, [9]Department of Earth and Space Sciences, University of California, Los Angeles, CA, USA, [10]Southwest Research Institute, San Antonio, TX, USA

Abstract Cold ions of ionospheric origin are present throughout the Earth's magnetosphere, including the dayside magnetopause, where they modify the properties of magnetic reconnection, a major coupling mechanism at work between the magnetosheath and the magnetosphere. We present Magnetospheric MultiScale (MMS) spacecraft observations of the reconnecting magnetopause with different amounts of cold ions and show that their presence reduces the Hall term in the Ohm's law. Then, we compare two particle-in-cell simulations, with and without cold ions on the magnetospheric side. The cold ions remain magnetized inside the magnetospheric separatrix region, leading to the reduction of the perpendicular currents associated with the Hall effect. Moreover, this reduction is proportional to the relative number density of cold ions. And finally, the Hall electric field peak is reduced along the magnetospheric separatrix owing to cold ions. This should have an effect on energy conversion by reconnection from electromagnetic fields to kinetic energy of the particles.

Plain Language Summary The magnetic field of Earth creates a natural boundary that isolates and protects us from the particles and fields coming from the Sun, typically known as the solar wind. This natural shield is called the magnetosphere and is filled by plasma. The particles are coming from the solar wind and are usually deviated around the magnetosphere. However, various mechanisms are capable of interconnecting these two regions of plasma, permitting the exchange of mass and energy. Magnetic reconnection is a primary coupling mechanism and the driver of storms and substorms inside the magnetosphere. In this work, we investigate what occurs when particles of very low energy (cold ions) of ionospheric origin reach the reconnecting boundary between the solar wind and the magnetosphere. We use both spacecraft observations and numerical simulations, and we find that they modify the way reconnection operates, by reducing the currents carried by electrons. The electric fields associated with energization of particles are reduced as well under the presence of cold ions coming from the ionosphere.

1. Introduction

Magnetic reconnection is the main coupling mechanism between the solar wind and the Earth's magnetosphere. It is known to occur at the magnetopause where the two plasmas collide, with a reconnection rate that depends on local parameters such as magnetic field and plasma density (Cassak & Shay, 2007). Cold plasma (few electron volts) is typically found in different regions of the magnetosphere (André & Cully, 2012; Chappell et al., 1987), including the magnetopause boundary layer (Chen & Moore, 2006; Sauvaud et al., 2001; Walsh et al., 2014). There are different mechanisms that make this cold plasma component escape from the

ionosphere and populate the Earth's magnetosphere. The first mechanism is often referred as ionospheric outflows (e.g., Moore et al., 1997; Yau et al., 2007), where the cold plasma escapes directly along magnetic field lines in the polar regions, and the characteristic energy of the cold ions is below 10 eV. The second cold population is called the warm plasma cloak (Chappell et al., 2008), which is made of cold plasma of ionospheric origin from the nightside magnetosphere transported to the dayside magnetosphere via convection. It has characteristic energies ranging from few electron volts to hundreds of electron volts. Finally, erosion of the plasmasphere is another source of cold plasma for the magnetosphere. It is often observed in the form of plasmaspheric winds (Dandouras, 2013; Lemaire & Schunk, 1992) and plasmaspheric drainage plumes (Olsen et al., 1987). The plasmaspheric drainage plumes generate the largest number densities in the outer magnetosphere (up to 10–100 cm^{-3}), with energies of only a few electron volts (André & Cully, 2012; Walsh et al., 2014).

It has been shown that the cold plasma component can mass load the magnetospheric side of the reconnecting boundary and reduce the reconnection rate (Borovsky et al., 2013; Walsh et al., 2013). This mass loading can lead, for extreme cases, to a magnetospheric density enhancement of up to 3 orders of magnitude (from ~0.1 to ~100 cm^{-3}; Walsh et al., 2014).

In addition to the mass loading effect, recent observations and simulations have shown that cold ions introduce new microphysical effects to magnetic reconnection when in nonnegligible proportion, owing to their smaller gyroradius. André et al. (2010) observed cold ions inside the separatrix region of magnetic reconnection using in situ spacecraft measurements and suggested that they could remain magnetized and $\mathbf{E} \times \mathbf{B}$ drift inside this region. Later, it was shown that the cold ions could remain magnetized inside the separatrix and diffusion regions, as opposed to hot magnetospheric and magnetosheath ions (André et al., 2016; Toledo-Redondo, André, Khotyaintsev, et al., 2016; Toledo-Redondo et al., 2015). These works speculated that the drifting cold ions should reduce the perpendicular currents and therefore the $\mathbf{j} \times \mathbf{B}/en$. However, in situ observations cannot easily prove or quantify this effect, owing to the different conditions of each separatrix crossing and the local nature of these kind of observations, which make comparison of events a challenging task. To account for the partial demagnetization of ions, these previous works considered a three-population plasma: electrons, cold ions, and hot ions. The Ohm's law can be rewritten as follows, after neglecting the electron inertial term and considering that a steady state has been reached:

$$\mathbf{E} = \frac{1}{en}\mathbf{j} \times \mathbf{B} - \frac{1}{en}\nabla \cdot \mathbf{P_e} - \frac{n_{ih}}{n}\mathbf{v}_{ih} \times \mathbf{B} - \frac{n_{ic}}{n}\mathbf{v}_{ic} \times \mathbf{B}, \quad (1)$$

with $\mathbf{E}$ and $\mathbf{B}$ the electric and magnetic fields, $\mathbf{j}$ the current density, $\mathbf{P_e}$ the electron pressure tensor, n the number density, and subscripts ih and ic standing for hot and cold ions, respectively.

It has been also found that cold ions are not only accelerated by being picked up by the reconnection jet but also heated while crossing the magnetospheric separatrix. The heating mechanisms have been related to waves and electric field gradients present in the separatrix region, and the cold ion heating can take a significant fraction of the energy budget that magnetic reconnection transfers to the particles (Toledo-Redondo et al., 2017; Toledo-Redondo, André, Vaivads, et al., 2016). The interaction between magnetosheath ions and cold magnetospheric ions at the separatrix region can lead to the generation of lower hybrid drift waves via the ion-ion cross-field instability, which in turn can heat the cold ions (Graham et al., 2017; Toledo-Redondo et al., 2017). However, Li et al. (2017) reported observations of cold ions that remained cold inside the reconnection exhaust.

Moreover, cold ions can play a role in sustaining the Larmor electric field (Malakit et al., 2013) far away from the X line once reconnection starts (Dargent et al., 2017). Again, the smaller gyroradius of the cold ions allow them to $\mathbf{E} \times \mathbf{B}$ drift inside the Larmor $\mathbf{E}$ field structure, sustaining any preexisting electric field. This means that the presence of cold ions precludes the observation of such a Larmor electric field as a tracer of the spacecraft proximity to the X line.

An interesting point is whether cold ions have an effect on the reconnection rate owing to their lower temperature. Recent simulations with a moderate amount of cold ions have reported that they do not have a significant extra effect on the reconnection rate once the mass loading effect is accounted for, that is, the normalized reconnection rate is not changed by cold ions (Dargent et al., 2017; Divin et al., 2016).

A remaining open question concerns the perpendicular current reduction inside the separatrix region and whether this has an effect on the Hall electric field and its associated potential drop across the boundary. In

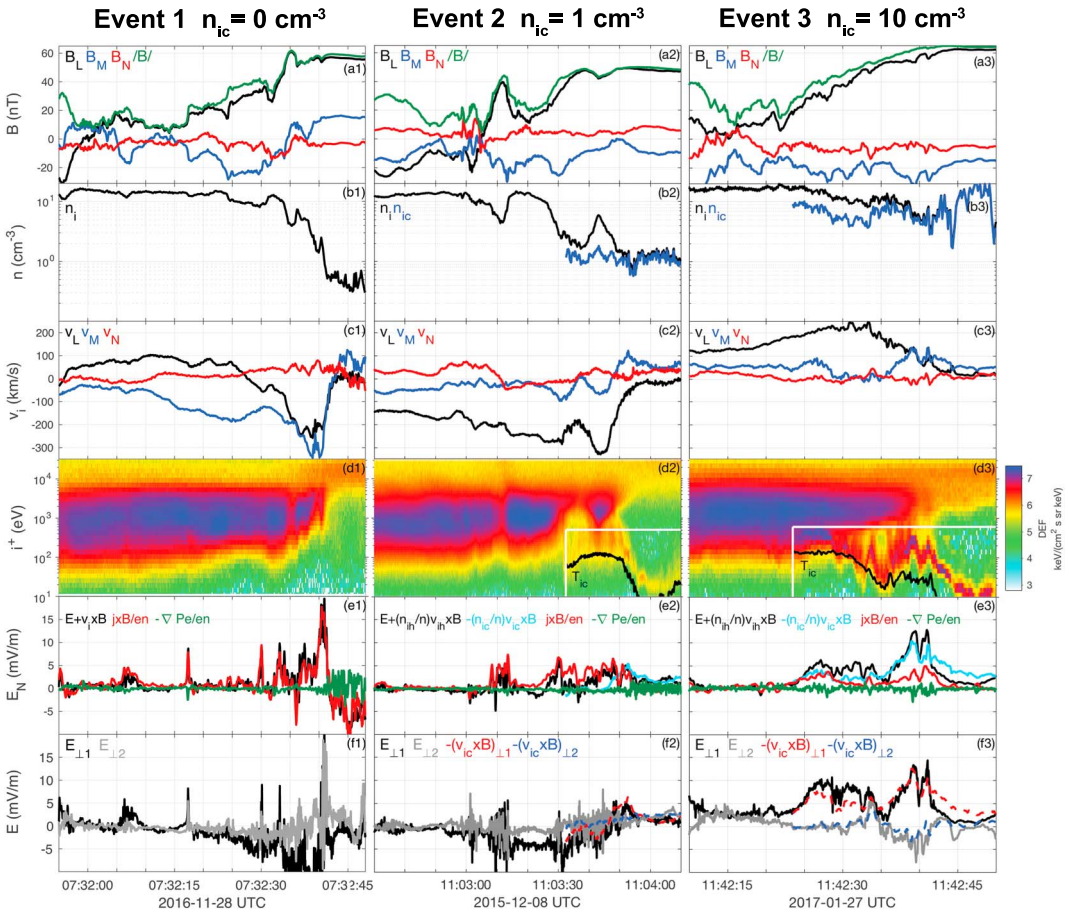

Figure 1. MMS1 observations of three magnetopause crossings with different amounts of cold ions on the magnetospheric side. (a1–a3) Magnetic field measured by FGM in LMN coordinates. (b1–b3) Total (black) and cold (blue) ion densities observed by FPI. (c1–c3) Ion velocities from FPI in LMN coordinates. (d1–d3) Ion differential energy flux spectrograms observed by FPI. White rectangles mark the portion of the data used to compute the cold ion moments. Black lines correspond to cold ion Temperature. (e1–e3) *N* component of the Ohm's law terms calculated using MMS data. *j* and ∇P_e are computed using four spacecraft techniques. (f1–f3) Comparison of $\mathbf{E}_\perp$ and $-(\mathbf{v}_{ic} \times \mathbf{B})_\perp$.

this work, we study the effects of a moderate amount of cold ions on magnetic reconnection at the dayside magnetopause. We focus in particular on the $\mathbf{j} \times \mathbf{B}/en$ term reduction and whether it has an impact on the Hall electric field. This electric field is important for particle energization, because it constitutes a potential drop of up to several kilovolts (e.g., Aunai et al., 2011; Khotyaintsev et al., 2006; Toledo-Redondo et al., 2015; Wygant et al., 2005). The paper is structured as follows: section 2 shows three examples of spacecraft observations of the reconnecting magnetopause with different amounts of cold ions. Section 3 describes the simulation setup used for this investigation. Section 4 presents the results of the simulations, comparing the two main runs (with and without cold ions). Section 5 discusses the implications of the results and summarizes the findings.

2. Spacecraft Observations of Dayside Reconnection With Cold Ions

The MMS mission was launched in 2015 with the specific aim of studying magnetic reconnection. It is composed of four identical spacecraft flying in tetrahedron configuration during the orbit's apogee. It carries a suite of in situ instrumentation to measure the fields and particle properties, and it has been designed to resolve down to the electron scales of the plasma (e.g., Burch et al., 2016; Lavraud et al., 2016). In this work, we use data from the flux gate magnetometer (Russell et al., 2016) to measure the magnetic field, the spin double probe (Lindqvist et al., 2014) and the axial double probe (Ergun et al., 2016) to measure electric fields, and the fast plasma investigation (Pollock et al., 2016) to measure ion and electron distribution functions.

We selected three independent magnetopause crossings made by the MMS spacecraft mission in the subsolar region, with different amounts of cold ions of ionospheric origin on the magnetospheric side (Figure 1). The

magnetopause crossings can be identified as **B** field rotations (Figures 1a1–1a3). The LMN coordinates are obtained from applying minimum variance analysis to the magnetic field as it rotates from the magnetosheath to the magnetosphere, and their coordinates are roughly **L** ≃ **Z**, **M** ≃ −**Y**, and **N** ≃ **X** in GSE. The exact LMN coordinates are specified in Table S1 of the supporting information.

Total ion densities (n_i) and cold ion densities (n_{ic}) are plotted in Figures 1b1–1b3 using black and blue lines, respectively. Event 1 has no cold ions of ionospheric origin, event 2 has a moderate amount of cold ions on the magnetospheric side (an average of 1.1 cm^{-3}), and event 3 has a large amount of cold ions on the magnetospheric side (an average of 11.1 cm^{-3}). For event 3, the magnetospheric and magnetosheath densities are of the same order of magnitude (11.1 and 16.3 cm^{-3}, respectively).

Figures 1c1–1c3 show the ion velocities ($\mathbf{v}_i$) measured by fast plasma investigation. Outflow jets are observed inside the current sheet for the three events and are consistent with ongoing reconnection. The omnidirectional differential energy fluxes for ions are shown in Figures 1d1–1d3. On the magnetospheric side, the ring current ion populations exhibit temperatures (T_{ih}) on the order of several kiloelectron volts (3.9, 6.1, and 4.6 keV for events 1–3, respectively). The cold ions of events 2 and 3 have temperatures (T_{ic}) of roughly 10 eV in the magnetosphere and are heated in the separatrix up to few hundred electron volts (black curves in Figures 1d2 and 1d3), consistent with previous cold ion heating studies (Toledo-Redondo et al., 2017). Magnetosheath ions have temperatures (T_{is}) of several hundred electron volts (540, 440, and 790 eV for events 1–3, respectively). The white lines in Figures 1d2 and 1d3 mark the part of the spectrogram used for cold ion density (n_{ic}), velocity (v_{ic}), and temperature (T_{ic}) calculations.

Figures 1e1–1e3 show the *N* component of the different Ohm's law terms (see equation (1). The largest $(\mathbf{E} + \mathbf{v}_i \times \mathbf{B})_N$ and $(\mathbf{j} \times \mathbf{B}/en)_N$ terms are observed in event 1, when no cold ions are present, and they roughly balance each other (Khotyaintsev et al., 2006). For events 2 and 3, cold ions remain roughly frozen-in inside the Hall **E** field region (see Figures 1f2 and 1f3) and contribute to the balance of the Ohm's law (cyan curves in Figures 1e2 and 1e3); see Toledo-Redondo et al. (2015) and André et al. (2016). This effect is particularly dramatic for event 3 when many cold ions are present at the reconnecting boundary. Finally, the contributions of the electron pressure gradient term are roughly 1 order of magnitude smaller than the other terms for the three events.

3. Simulation Setup

We use 2.5-D fully kinetic particle-in-cell model to simulate the reconnecting magnetopause at Earth, based on the SMILEI code (Derouillat et al., 2018). The same simulations have been previously used and described in Dargent et al. (2017). The magnetic field and density units of the simulation are normalized to magnetosheath parameters. The mass, charge, time, and distance are normalized to magnetosheath ion parameters (proton mass, proton charge, inverse of the proton gyrofrequency, and proton inertial length, respectively). The **B**, n, and T_i ratios between the magnetosphere and the magnetosheath have been chosen based on spacecraft observations in the subsolar magnetopause region (Toledo-Redondo et al., 2017, 2015) and are described in Tables S2 and S3 of the supporting information. The magnetospheric magnetic field is 2 times larger in magnitude and antiparallel to the magnetosheath magnetic field. The plasma density of the magnetosphere is one third of the magnetosheath density. We make use of two simulations, where one of them includes cold ions on the magnetospheric side. The global plasma parameters of the magnetosphere and magnetosheath (**B**, n, T_i, T_e) remain equal in both simulations, to facilitate their comparison. The only difference between run 1 (run without cold ions) and run 2 (run with cold ions) is the magnetospheric ion distribution function. For run 2 we have included two populations: cold magnetospheric ions representing two thirds of the magnetospheric density and hot magnetospheric ions representing one third of the magnetospheric density. The hot to cold ion temperature ratio in the magnetosphere is set to be 500, consistent with previous observations at the subsolar magnetopause. Therefore, the hot ion temperature in run 2 is higher than that in run 1 so that the total ion pressure on the magnetosphere remains the same on the two runs. More details can be found in Figure S1 and Tables S2 and S3 of the supporting information. The total ion to electron temperature ratio is set to 5. The mass ratio between ions and electrons is chosen to be 25, to make the computations feasible. After $t = 120$, the simulation is considered to be in steady state. The simulation without cold ions, or run 1, roughly corresponds to the conditions of event 1 in Figure 1, while the simulation with cold ions, or run 2, roughly corresponds to the conditions of event 2 in Figure 1.

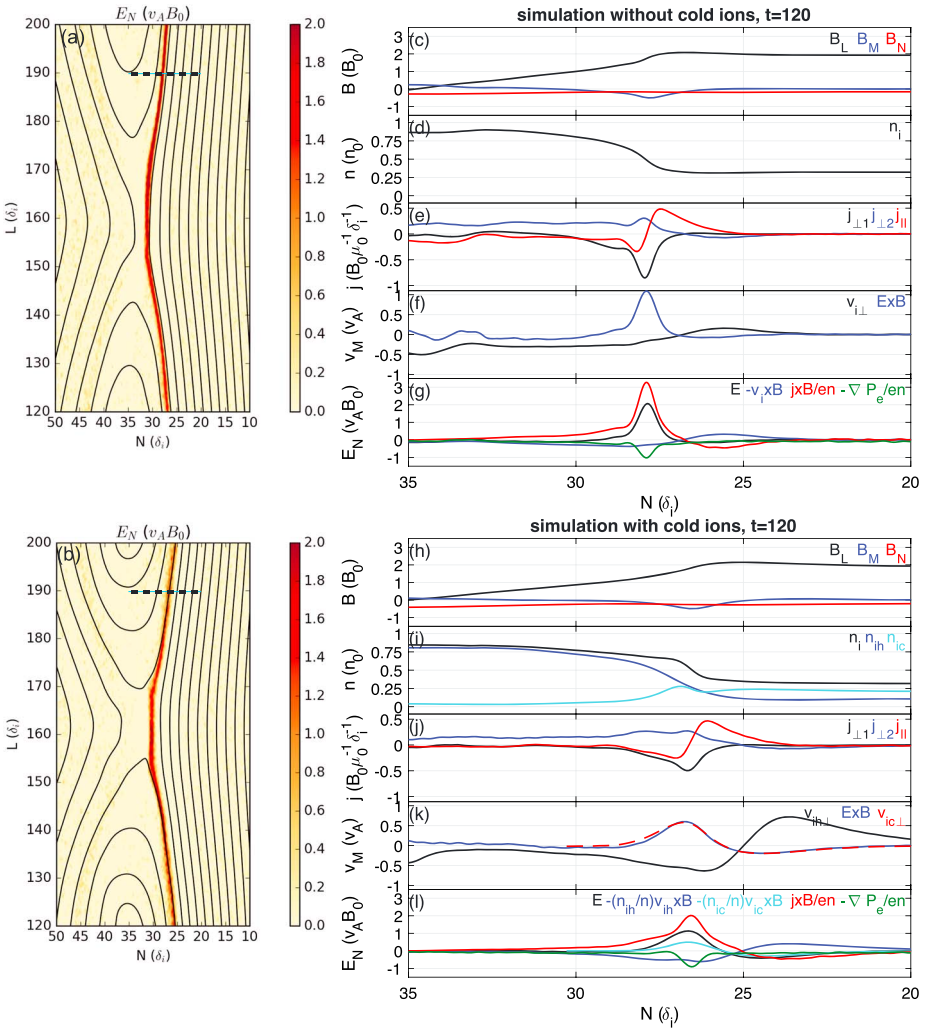

Figure 2. Single trajectories comparison of the simulations with and without cold ions. (a) Normal electric field (E_N) at $t = 120$ for the simulation without cold ions. The virtual spacecraft trajectory used in Figures 2c-2g is plotted in black. (b) Normal electric field (E_N) at $t = 120$ for the simulation with cold ions. The virtual spacecraft trajectory used in Figures 2h–2l is plotted in black. (c) Magnetic field along the trajectory $L = 190$ for the simulation without cold ions. (d) Total ion density. (e) Current density in field-aligned coordinates. (f) *M* component of the perpendicular ion velocity compared to $\mathbf{E} \times \mathbf{B}$. (g) Ohm's law terms. (h) Magnetic field along the trajectory $L = 190$ for the simulation with cold ions. (i) Total (i), hot (ih), and cold (ic) ion densities. (j) Current density in field-aligned coordinates. (k) *M* component of the perpendicular total (i) and cold (ic) ion velocity compared to $\mathbf{E} \times \mathbf{B}$. (l) Ohm's law terms.

4. Simulation Results

In this section, we compare the results from the two simulations, with and without cold ions. We focus on the microphysics occurring inside the thin structure of large E_N, or Hall **E** field, inside the magnetospheric separatrix region. This layer can be observed in red in Figures 2a and 2b, which correspond to E_N at $t = 120$ for runs without and with cold ions, respectively. The width (extent along **N**) of the structure is on the order of few magnetosheath ion inertial lengths. Figures 2c–2g and 2h–2l correspond to different quantities along the black dashed trajectories marked in Figures 2a and 2b, for a fixed time $t = 120$, which recall the MMS trajectories of the events of Figure 1. The **L**, **M**, and **N** coordinates of Figure 2 correspond to the **X**, -**Y**, and **Z** coordinates of the simulation box.

Figures 2c and 2h show the **B** field for the two trajectories, which is roughly the same. Figure 2d shows the total ion density (n_i, magnetospheric plus magnetosheath ions), and it is roughly equal to the total ion density of Figure 2i. In Figure 2i, the cold magnetospheric ion density, n_{ic}, and the hot magnetospheric plus magnetosheath, n_{ih}, are also shown. Cold and hot ions are flagged in the simulation setup with cold ions, and

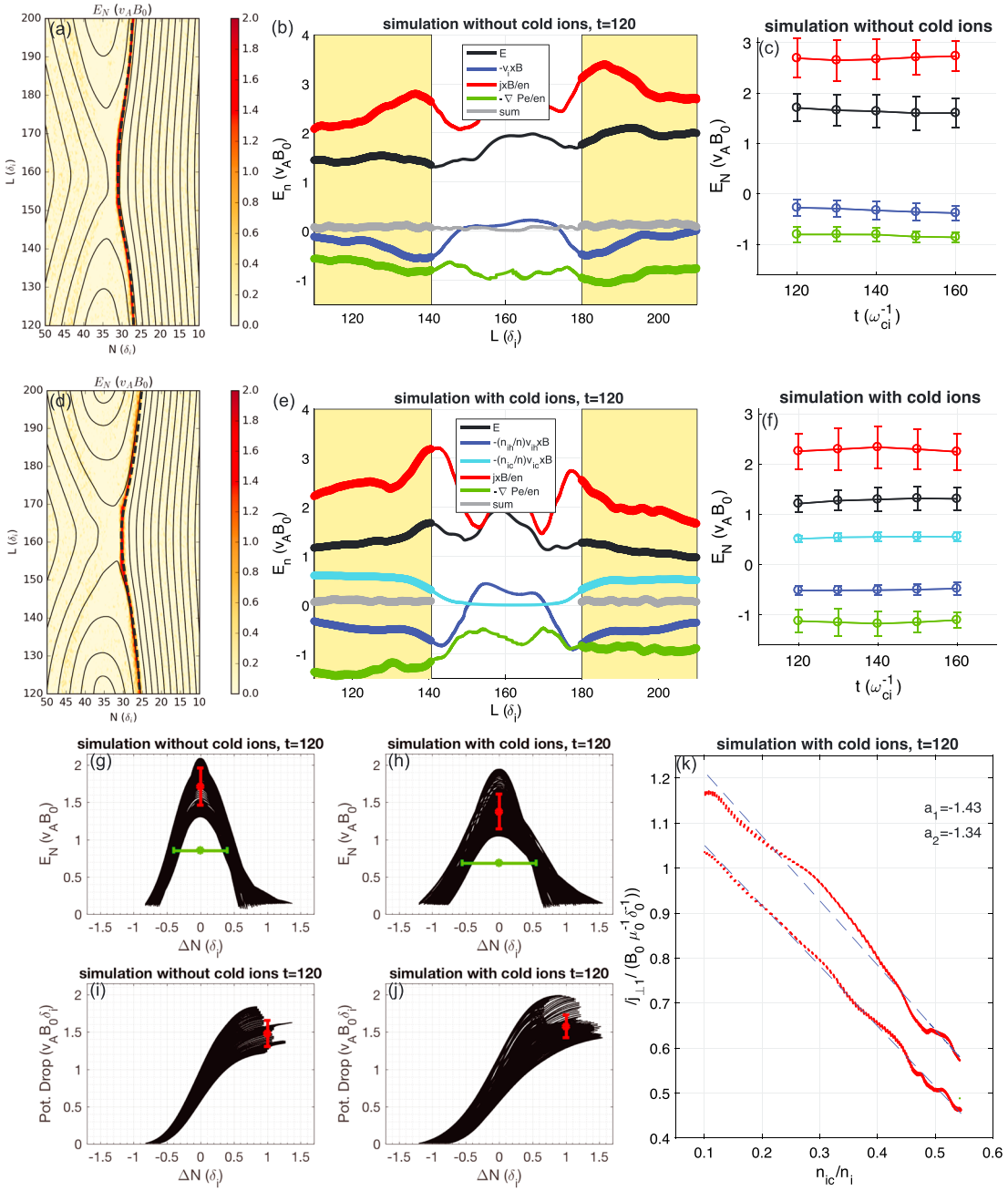

Figure 3. Ohm's law terms along the maximum Hall electric field. (a) Normal electric field (E_N) at $t = 120$ for the simulation without cold ions. The virtual spacecraft trajectory used in panel (b) is plotted in black, and it follows the maximum E_N. (b) Ohm's law terms along the trajectory that follows the maximum E_N for the simulation without cold ions. (c) Averaged Ohm's law terms in the separatrices for the simulation without cold ions as a function of time. Error bars represent one standard deviation. (d–f) Same as a–c for the simulation with cold ions. (g) Hall electric field statistics for the simulation without cold ions. (h) Hall electric field statistics for the simulation with cold ions. (i) Potential drop statistics for the simulation without cold ions. (j) Potential drop statistics for the simulation with cold ions. (k) $j_{\perp 1}$ as a function of the relative cold ion density (n_{ic}/n_i).

therefore, their partial moments can be obtained at any time and location of the simulation box. Figures 2e and 2j show the current density in field-aligned coordinates for the two runs, where the ⊥1 direction roughly corresponds to **M** and the ⊥2 direction to **N**. $j_{\perp 1}$ has a minimum at −0.85 for the run without cold ions and at −0.5 for the run with cold ions, indicating a reduction of the perpendicular current owing to the cold ions, consistent with recent findings using Cluster and MMS observations (André et al., 2016; Toledo-Redondo et al., 2015). Figure 2f compares the **M** component of the **E**×**B** velocity and the perpendicular ion velocity, $v_{i\perp}$, showing that the ions are not frozen-in inside the Hall **E** region. On the other hand, we show that cold ions remain

frozen-in and therefore $\mathbf{E}\times\mathbf{B}$ drift inside the region (red curve in Figure 2k), as opposed to hot magnetospheric and magnetosheath ions (black curve), which are accelerated by E_N as they cross the separatrix region. The finite gyroradius effects of the hot magnetospheric and magnetosheath ions (black curves in Figures 2f and 2k) result in positive and negative v_M ion velocities, respectively; see also Phan et al. (2016). This effect is larger for the simulation with cold ions, owing to the larger temperature of the hot magnetospheric ions imposed in this simulation and a sharper density gradient in the separatrix boundary (Figure 2i).

Finally, Figures 2g and 2l show the **N** component Ohm's law terms across the Hall **E** field region. In the run without cold ions, that is, Figure 2g, $(\mathbf{E}+\mathbf{v}_i\times\mathbf{B})_N$ roughly equals $(\mathbf{j}\times\mathbf{B}/en)_N$ as in Figure 1e1; see also Khotyaintsev et al. (2006) and Vaivads et al. (2004). However, a nonnegligible $-(\nabla\mathbf{P}_e/en)_N$ term is also present and has to be accounted for in our simulations for balancing equation (1), which is not observed in spacecraft measurements. We attribute this deviation from observations to the nonrealistic mass ratio between ions and electrons, which artificially enhances the magnitude of the electron pressure gradient term. On the other hand, for run 2 (Figure 2l), the term $-(n_{ic}/n)(\mathbf{v}_{ic}\times\mathbf{B})_N$ contributes to balance the Ohm's law as in Figure 1e2, and the peak values of E_N and $(\mathbf{j}\times\mathbf{B}/en)_N$ are smaller than in the simulation without cold ions.

Spacecraft observations of magnetic reconnection can only make observations locally across a trajectory when crossing the reconnecting current sheet, similar to the data shown in Figure 2. Simulations, however, offer a full picture of the phenomenon and can help us understand the large-scale impact of cold ion microphysics. To understand how the cold ions affect the Hall physics, we computed the Ohm's law terms along the Hall **E** field structure for the simulation box, at $t = 120$. In particular, we traced the maximum E_N along the **L** direction (dashed black lines in Figures 3a and 3d) and computed the different Ohm's law terms of equation (1). The results are shown in Figures 3b and 3e. As we move far away from the X line, the reconnection jets develop and broaden.

Next, we average the different terms along **L** inside the simulation box. The cold ion density is small in the center of the box, owing to $\mathbf{E}\times\mathbf{B}$ motion at scales that do not affect hot ions and accelerate them away from the diffusion region. We have highlighted in Figures 3b and 3e using yellow color the regions where the cold ion density term is at least 50% of its maximum value in the simulation with cold ions; these are the regions used for the averaging and comparison that are explained below. We compare the averaged Ohm's law terms along the yellow shaded separatrices marked in Figures 3b and 3e and show the results in Figures 3c and 3f, at times $t = 120$, 130, 140, 150, and 160. The error bars correspond to one standard deviation of the variations along the magnetospheric separatrices. The results at different times after $t = 120$ remain roughly constant, showing the steady state reached by the simulation. We also plotted Figures 3b and 3e at different times between 120 and 160 and found no significant differences. The E_N term (black) and $(\mathbf{j}\times\mathbf{B}/en)_N$ term (red) are smaller on average for the simulation with cold ions.

In Figures 3g and 3h we plot E_N for all the horizontal trajectories between $\mathbf{L} = [120, 200]$ at steps of 0.5 δ_i using black lines, for the simulations without and with cold ions, respectively. The red dots indicate the averaged maximum E_N, and the red error bars correspond to one standard deviation, while the green error bars indicate the averaged width at half the maximum E_N value. The maximum value of the Hall electric field is larger in the run without cold ions than in the run with cold ions (see also black curves in Figures 3e and 3f). On the other hand, the Hall electric field region becomes broader in the simulation with cold ions. Figures 3i and 3j show the corresponding potential drops across the Hall electric field region for each trajectory using black lines and their averaged values and one standard deviations using red dots and error bars, respectively. We find that the averaged potential drops are roughly equal.

The $(\mathbf{j}\times\mathbf{B}/en)_N$ reduction is caused by a reduction in $j_{\perp1}$, while **B** and n remain similar among the two simulations (not shown). We provide further evidence of the perpendicular current reduction owing to cold ions in Figure 3k, where the $j_{\perp1}$ values along the dashed black trajectory in Figure 3d are plotted as a function of the relative amount of cold ions (n_{ic}/n_i) using red dots. The blue lines correspond to two linear fits of the data for the downward and upward jets, and their slopes are indicated as a_1 and a_2, respectively. A linear decrease in $j_{\perp1}$ as a function of the relative cold ion density is found, and we can conclude that the cold ions effectively reduce the perpendicular currents along the magnetospheric separatrix. On the other hand, when the potential drop associated to $(\mathbf{j}\times\mathbf{B}/en)_N$ is compared between the two simulations, they remain roughly equal, as shown for E_N in Figures 3i and 3j. Like with E_N, this occurs owing to a broader $(\mathbf{j}\times\mathbf{B}/en)_N$ region that compensates the lower value of **j**. Since the pressure balance and therefore the integrated term $\nabla(\mathbf{P}_i+\mathbf{P}_e)$ is set to be equal among the two simulations, the integrated $\mathbf{j}\times\mathbf{B}$ term must also remain equal.

5. Discussion and Conclusion

Previous in situ observations of magnetic reconnection reported that cold ions of magnetospheric origin could $\mathbf{E}\times\mathbf{B}$ drift inside the narrow structure of the Hall electric field and that this should have an effect on the perpendicular currents and the Hall electric field itself (André et al., 2016; Toledo-Redondo et al., 2015). We here bring evidence of this current and Hall electric field peak reduction by comparing two simulations, with and without cold ions, where the global parameters of the inflow regions, that is, plasma density, temperature, and magnetic field, remain the same.

It is found that the presence of cold ions effectively reduces the perpendicular currents inside the Hall electric field region along the separatrices (Figure 3k), resulting in a reduced $\mathbf{j}\times\mathbf{B}/en$ term (Figures 3c and 3f). The reduction of the perpendicular currents and the modification of the relative ion-ion drift speeds can have a direct effect over the microinstabilities that can develop. Graham et al. (2017) showed that the presence of cold ions at the magnetopause favored the generation of lower hybrid drift waves via an ion-ion instability. In addition, a reduction of the current carried by electrons should have implications for instabilities that are dependent on the current, such as, for instance, the Buneman instability. Another implication of the current reduction owing to cold ion presence can be noticed by looking at Figures 1e1–1e3. When no cold ions are present (event 1), $\mathbf{E}\simeq\ \mathbf{j}\times\mathbf{B}/en$ ($\mathbf{v}_i\times\mathbf{B}$ term is small); see also Khotyaintsev et al. (2006). On the other hand, when cold ions are present, and in particular for large amounts of them, $\mathbf{E}\neq\ \mathbf{j}\times\mathbf{B}/en$, and therefore, one term cannot be used as a proxy of the other in spacecraft observations when cold ions are present.

An important question is whether this current reduction has an impact over the Hall electric field. This field extends along the magnetospheric separatrix region, separating the inflow region from the exhaust. It represents a potential drop of several kilovolts (Khotyaintsev et al., 2006) and plays an important role energizing the particles which cross that boundary. A reduction of this electric field should have large-scale consequences on the jet formation, evolution, and energy conversion from the fields to the particles. In our simulation with cold ions, a reduction of the Hall electric field peak value is found in the simulation with cold ions (Figures 3g and 3h). On the other hand, the integrated potential drop across the Hall electric field region remains roughly equal in the two simulations (Figures 3i and 3j). While the maximum E_N and $\mathbf{j}_\perp$ are reduced in the simulation with cold ions, the Hall electric field region becomes broader in the **N** direction. The two effects compensate each other, maintaining the integrated potential drop roughly equal. However, in a real situation, the hot magnetospheric ions have similar temperatures regardless of the amount of cold ions present at the separatrix region. Under this situation, we expect an effective decrease of the potential drop across the separatrix owing to the reduction of the Hall effect, as the MMS observations suggest by comparing the black curves in Figures 1e1–1e3. This effect would reduce the ability of magnetic reconnection to energize the magnetospheric ions when crossing from the inflow to the exhaust region. Future simulations including the impact of a cold ion plume on the reconnecting magnetopause will help us understand the reduction of the Hall electric field and the implications for plasma energization by reconnection, as well as the connection of this electric field with the reduction of the reconnection rate owing to mass loading of the magnetosphere.

To conclude, we investigated magnetic reconnection at the dayside magnetopause under the influence of cold ions of ionospheric origin using full particle-in-cell simulations and spacecraft observations. The two approaches show that cold ions behave differently from hot ions at the separatrices and have different relative motions. When cold ions are present in the Hall electric field region, the $\mathbf{v}_i\times\mathbf{B}$ term corresponds to the center of mass motion of the plasma and corresponds to an average motion between the two populations, but none of the populations really moves with $\mathbf{v}_i$. Cold ions $\mathbf{E}\times\mathbf{B}$ drift together with electrons and cancel out a portion of the perpendicular currents. This phenomenon is extended along the separatrices and reduces the Hall effect on a global scale. The relative ion drifts plus $\mathbf{j}_\perp$ reduction affects the type of instabilities that can arise in the separatrix region. Finally, the maximum value of the Hall electric field is reduced in the simulation and in the spacecraft observations with cold ions, and we expect this effect to have implications for plasma energization by magnetic reconnection.

Acknowledgments
We thank all the people involved in the MMS project for the high-quality data provided. We acknowledge support from the ISSI's international team *MMS and CLUSTER observations of magnetic reconnection* and from the Science faculty of the European Space Astronomy Centre (ESAC). This work was granted access to the HPC resources of IDRIS under the allocation i2015047231. The MMS data used in this work are available to the public in the MMS Science Data Center (https://lasp.colorado.edu/mms/sdc/public/). The simulation data are taken from Dargent et al. (2016) and Dargent et al. (2017).

References

André, M., & Cully, C. M. (2012). Low-energy ions: A previously hidden solar system particle population. *Geophysical Research Letters*, *39*, L03101. https://doi.org/10.1029/2011GL050242

André, M., Li, W., Toledo-Redondo, S., Khotyaintsev, Y. V., Vaivads, A., Graham, D. B., et al. (2016). Magnetic reconnection and modification of the hall physics due to cold ions at the magnetopause. *Geophysical Research Letters*, *43*, 6705–6712. https://doi.org/10.1002/2016GL069665

André, M., Vaivads, A., Khotyaintsev, Y. V., Laitinen, T., Nilsson, H., Stenberg, G., et al. (2010). Magnetic reconnection and cold plasma at the magnetopause. *Geophysical Research Letters*, *37*, L22108. https://doi.org/10.1029/2010GL044611

Aunai, N., Belmont, G., & Smets, R. (2011). Proton acceleration in antiparallel collisionless magnetic reconnection: Kinetic mechanisms behind the fluid dynamics. *Journal of Geophysical Research*, *116*, A09232. https://doi.org/10.1029/2011JA016688

Borovsky, J. E., Denton, M. H., Denton, R. E., Jordanova, V. K., & Krall, J. (2013). Estimating the effects of ionospheric plasma on solar wind/magnetosphere coupling via mass loading of dayside reconnection: Ion-plasma-sheet oxygen, plasmaspheric drainage plumes, and the plasma cloak. *Journal of Geophysical Research: Space Physics*, *118*, 5695–5719. https://doi.org/10.1002/jgra.50527

Burch, J. L., Moore, T. E., Torbert, R. B., & Giles, B. L. (2016). Magnetospheric multiscale overview and science objectives. *Space Science Reviews*, *199*, 1–17. https://doi.org/10.1007/s11214-015-0164-9

Cassak, P., & Shay, M. (2007). Scaling of asymmetric magnetic reconnection: General theory and collisional simulations. *Physics of Plasmas (1994-present)*, *14*(10), 102114.

Chappell, C. R., Huddleston, M. M., Moore, T. E., Giles, B. L., & Delcourt, D. C. (2008). Observations of the warm plasma cloak and an explanation of its formation in the magnetosphere. *Journal of Geophysical Research*, *113*, A09206. https://doi.org/10.1029/2007JA012945

Chappell, C. R., Moore, T. E., & Waite, J. H. (1987). The ionosphere as a fully adequate source of plasma for the Earth's magnetosphere. *Journal of Geophysical Research*, *92*(A6), 5896–5910. https://doi.org/10.1029/JA092iA06p05896

Chen, S.-H., & Moore, T. E. (2006). Magnetospheric convection and thermal ions in the dayside outer magnetosphere. *Journal of Geophysical Research*, *111*, A03215. https://doi.org/10.1029/2005JA011084

Dandouras, I. (2013). Detection of a plasmaspheric wind in the Earth's magnetosphere by the cluster spacecraft. *Annales de Geophysique*, *31*, 1143–1153.

Dargent, J., Aunai, N., Belmont, G., Dorville, N., Lavraud, B., & Hesse, M. (2016). Full particle-in-cell simulations of kinetic equilibria and the role of the initial current sheet on steady asymmetric magnetic reconnection. *Journal of Plasma Physics*, *82*(3), 90582305. https://doi.org/10.1017/S002237781600057X

Dargent, J., Aunai, N., Lavraud, B., Toledo-Redondo, S., Shay, M., Cassak, P., & Malakit, K. (2017). Kinetic simulation of asymmetric magnetic reconnection with cold ions. *Journal of Geophysical Research: Space Physics*, *122*, 5290–5306. https://doi.org/10.1002/2016JA023831

Derouillat, J., Beck, A., Pérez, F., Vinci, T., Chiaramello, M., Grassi, A., et al. (2018). Smilei : A collaborative, open-source, multi-purpose particle-in-cell code for plasma simulation. *Computer Physics Communications*, *222*, 351–373. https://doi.org/10.1016/j.cpc.2017.09.024

Divin, A., Khotyaintsev, Y. V., Vaivads, A., André, M., Toledo-Redondo, S., Markidis, S., & Lapenta, G. (2016). Three-scale structure of diffusion region in the presence of cold ions. *Journal of Geophysical Research: Space Physics*, *121*, 12,001–12,013. https://doi.org/10.1002/2016JA023606.

Ergun, R., Tucker, S., Westfall, J., Goodrich, K., Malaspina, D., Summers, D., et al. (2016). The axial double probe and fields signal processing for the MMS mission. *Space Science Reviews*, *199*(1-4), 167–188.

Graham, D. B., Khotyaintsev, Y. V., Norgren, C., Vaivads, A., André, M., Toledo-Redondo, S., et al. (2017). Lower hybrid waves in the ion diffusion and magnetospheric inflow regions. *Journal of Geophysical Research: Space Physics*, *122*, 517–533. https://doi.org/10.1002/2016JA023572

Khotyaintsev, Y. V., Vaivads, A., Retinò, A. A., André, M., Owen, C. J., & Nilsson, H. (2006). Formation of inner structure of a reconnection separatrix region. *Physical Review Letters*, *97*(20), 205003.

Lavraud, B., Zhang, Y. C., Vernisse, Y., Gershman, D. J., Dorelli, J., Cassak, P. A., et al. (2016). Currents and associated electron scattering and bouncing near the diffusion region at Earth's magnetopause. *Geophysical Research Letters*, *43*, 3042–3050. https://doi.org/10.1002/2016GL068359

Lemaire, J., & Schunk, R. (1992). Plasmaspheric wind. *Journal of Atmospheric and Terrestrial Physics*, *54*(3), 467–477. https://doi.org/10.1016/0021-9169(92)90026-H

Li, W. Y., André, M., Khotyaintsev, Y. V., Vaivads, A., Fuselier, S. A., Graham, D. B., et al. (2017). Cold ionospheric ions in the magnetic reconnection outflow region. *Journal of Geophysical Research: Space Physics*, *122*, 10,194–10,202. https://doi.org/10.1002/2017JA024287JA024287

Lindqvist, P.-A., Olsson, G., Torbert, R. B., King, B., Granoff, M., Rau, D., et al. (2014). The spin-plane double probe electric field instrument for MMS. *Space Science Reviews*, *199*, 1–29. https://doi.org/10.1007/s11214-014-0116-9

Malakit, K., Shay, M. A., Cassak, P. A., & Ruffolo, D. (2013). New electric field in asymmetric magnetic reconnection. *Physical Review Letters*, *111*(13), 135001. https://doi.org/10.1103/PhysRevLett.111.135001

Moore, T., Chappell, C., Chandler, M., Craven, P., Giles, B., Pollock, C., et al. (1997). High-altitude observations of the polar wind. *Science*, *277*(5324), 349–351.

Olsen, R. C., Shawhan, S. D., Gallagher, D. L., Green, J. L., Chappell, C. R., & Anderson, R. R. (1987). Plasma observations at the Earth's magnetic equator. *Journal of Geophysical Research*, *92*(A3), 2385–2407. https://doi.org/10.1029/JA092iA03p02385

Phan, T. D., Shay, M. A., Haggerty, C. C., Gosling, J. T., Eastwood, J. P., Fujimoto, M., et al. (2016). Ion Larmor radius effects near a reconnection X line at the magnetopause: THEMIS observations and simulation comparison. *Geophysical Research Letters*, *43*, 8844–8852. https://doi.org/10.1002/2016GL070224

Pollock, C., Moore, T., Jacques, A., Burch, J., Gliese, U., Saito, Y., et al. (2016). Fast plasma investigation for magnetospheric multiscale. *Space Science Reviews*, *199*(1-4), 331–406.

Russell, C., Anderson, B., Baumjohann, W., Bromund, K., Dearborn, D., Fischer, D., et al. (2016). The magnetospheric multiscale magnetometers. *Space Science Reviews*, *199*, 1–68.

Sauvaud, J.-A., Lundin, R., Reme, H., McFadden, J., Carlson, C., Parks, G., et al. (2001). Intermittent thermal plasma acceleration linked to sporadic motions of the magnetopause, first cluster results. *Annales Geophysicae*, *19*, 1523–1532.

Toledo-Redondo, S., André, M., Khotyaintsev, Y. V., Lavraud, B., Vaivads, A., Graham, D. B., et al. (2017). Energy budget and mechanisms of cold ion heating in asymmetric magnetic reconnection. *Journal of Geophysical Research: Space Physics*, *122*, 9396–9413. https://doi.org/10.1002/2017JA024553

Toledo-Redondo, S., André, M., Khotyaintsev, Y. V., Vaivads, A., Walsh, A., Li, W., et al. (2016). Cold ion demagnetization near the X-line of magnetic reconnection. *Geophysical Research Letters*, *43*, 6759–6767. https://doi.org/10.1002/2016GL069877

Toledo-Redondo, S., André, M., Vaivads, A., Khotyaintsev, Y. V., Lavraud, B., Graham, D., et al. (2016). Cold ion heating at the dayside magnetopause during magnetic reconnection. *Geophysical Research Letters*, *43*, 58–66. https://doi.org/10.1002/2015GL067187

Toledo-Redondo, S., Vaivads, A., André, M., & Khotyaintsev, Y. V. (2015). Modification of the hall physics in magnetic reconnection due to cold ions at the Earth's magnetopause. *Geophysical Research Letters*, *42*, 6146–6154. https://doi.org/10.1002/2016GL069665

Vaivads, A., Khotyaintsev, Y., André, M., Retino, A., Buchert, S. C., Rogers, B. N., et al. (2004). Structure of the magnetic reconnection diffusion region from four-spacecraft observations. *Physical Review Letters*, *93*(10), 105001.

Walsh, B., Phan, T., Sibeck, D., & Souza, V. (2014). The plasmaspheric plume and magnetopause reconnection. *Geophysical Research Letters*, *41*, 223–228. https://doi.org/10.1002/2013GL058802

Walsh, B., Sibeck, D., Nishimura, Y., & Angelopoulos, V. (2013). Statistical analysis of the plasmaspheric plume at the magnetopause. *Journal of Geophysical Research: Space Physics*, *118*, 4844–4851. https://doi.org/10.1002/jgra.50458

Wygant, J., Cattell, C., Lysak, R., Song, Y., Dombeck, J., McFadden, J., et al. (2005). Cluster observations of an intense normal component of the electric field at a thin reconnecting current sheet in the tail and its role in the shock-like acceleration of the ion fluid into the separatrix region. *Journal of Geophysical Research*, *110*, 9206. https://doi.org/10.1029/2004JA010708

Yau, A. W., Abe, T., & Peterson, W. (2007). The polar wind: Recent observations. *Journal of Atmospheric and Solar-Terrestrial Physics*, *69*(16), 1936–1983. https://doi.org/10.1016/j.jastp.2007.08.010, recent Advances in the Polar Wind Theories and Observations.